Transonic and Supershear Crack Propagation Driven by Geometric Nonlinearities

Mohit Pundir,[1] Mokhtar Adda-Bedia,[2] and David S. Kammer[1,*]
[1]Institute for Building Materials, ETH Zurich, Switzerland
[2]Laboratoire de Physique, CNRS, ENS de Lyon, Université de Lyon, 69342 Lyon, France

(Received 18 August 2023; accepted 6 May 2024; published 31 May 2024)

Linear elastic fracture mechanics theory predicts that the speed of crack growth is limited by the Rayleigh wave speed. Although many experimental observations and numerical simulations have supported this prediction, some exceptions have raised questions about its validity. The underlying reasons for these discrepancies and the precise limiting speed of dynamic cracks remain unknown. Here, we demonstrate that tensile (mode I) cracks can exceed the Rayleigh wave speed and propagate at supershear speeds. We show that taking into account geometric nonlinearities, inherent in most materials, is sufficient to enable such propagation modes. These geometric nonlinearities modify the crack-tip singularity, resulting in different crack-tip opening displacements, cohesive zone behavior, and energy flows towards the crack tip.

DOI: 10.1103/PhysRevLett.132.226102

The speed at which cracks propagate is a fundamental characteristic that has implications in various fields such as material design [1], earthquake mechanics [2], and even the phenomenon of popping balloons [3]. Linear elastic fracture mechanics (LEFM) [4] plays a crucial role in predicting crack speed c_f by establishing an energy balance between the energy release rate, which drives crack growth, and the fracture energy (Γ), which resists it. This framework, which assumes that Γ is dissipated solely at the crack tip, predicts that the material Rayleigh wave speed c_R serves as a limiting speed for crack propagation. This prediction has been experimentally confirmed [5]. Crack growth occurring at speeds between c_R and the shear wave speed c_s is considered physically inadmissible, as it would generate energy rather than dissipate it. Nevertheless, LEFM predicts that cracks can propagate at supershear speeds $c_f > c_s$ if one assumes that dissipation occurs within a spatially extended zone around the crack tip [4,6]. However, the specific conditions that allow for supershear propagation of, particularly, opening (mode I) cracks and the processes involved in the transition through the forbidden speed range remain largely unknown.

Supershear crack growth is predominantly observed in cracks under shear (mode II) loading conditions, as described theoretically [7,8] and widely supported by numerical simulations [8–10], experimental studies [11–15], and natural observations [2,16–19]. Supershear propagation is generally associated with high-stress states [8,9]. In contrast, supershear propagation in cracks under mode I loading conditions is relatively rare. Molecular dynamics (MD) simulations [20,21] and lattice models [22–25] have shown instances of supershear crack speeds, while experimental observations have been reported for rubberlike materials [3,26,27], hydrogels [28] and structural materials where the loading is applied directly at the crack tip by some extreme conditions [29]. The presence of some type of nonlinearity, extending beyond the limits of LEFM, is a recurring feature in both simulations and experiments, indicating its potential contribution to enabling supershear growth in tensile cracks. However, the specific type of material nonlinearity required for this phenomenon, as well as its generality across different materials, remains unknown.

Here, we investigate the minimal requirements for the transition to supershear propagation of tensile cracks using numerical simulations. Our simulations reveal that the presence of geometric nonlinearities alone is the primary factor driving supershear crack growth resulting from a continuous acceleration through the transonic speed range. Since such nonlinearities are generally present in materials, these findings demonstrate that supershear propagation is an inherent characteristic in dynamic crack problems, independent of the specific material constitutive laws.

We consider the most generic and simple model without introducing a nonlinear material constitutive law or any additional material parameter. The material deformation is described by a two-dimensional plane-strain tensor E_{ij}, defined as

$$E_{ij} = \frac{1}{2}\left(\frac{\partial u_i}{\partial x_j} + \frac{\partial u_j}{\partial x_i} + \alpha \frac{\partial u_k}{\partial x_j}\frac{\partial u_k}{\partial x_i}\right), \tag{1}$$

where u_i and x_i are the ith displacement and coordinate component ($i \equiv x,\ y$), respectively. To easily switch between linear and geometrically nonlinear (GNL) cases, we introduce the factor $\alpha \in \{0, 1\}$. Therefore, for $\alpha = 1$, E_{ij} corresponds to the Green-Lagrangian strain tensor, while for $\alpha = 0$, it is its linear approximation, the infinitesimal

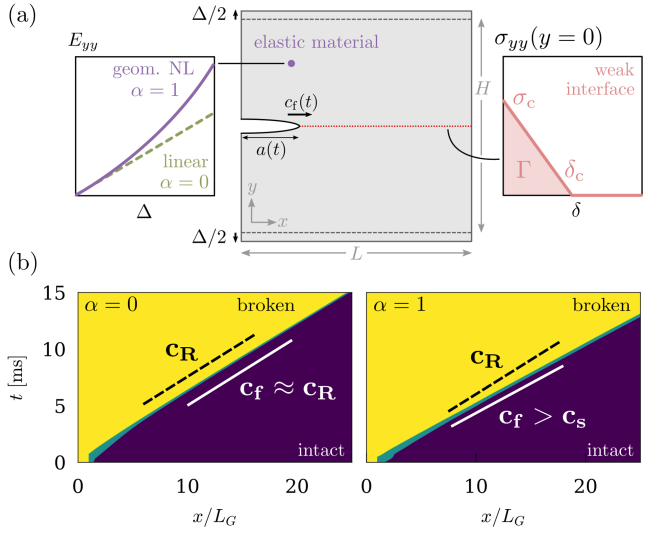

FIG. 1. Model setup and illustrative examples. (a) 2D model configuration with an elastic material and a weak cohesive interface. (b) Temporal evolution of interface for simulations at an imposed stretch $\lambda = 1.125$ with (left) linear elastic material ($\alpha = 0$) and (right) geometric nonlinear elastic material ($\alpha = 1$). Blue indicates intact material, turquoise the cohesive zone area, and yellow the broken interface. The crack speed c_f is indicated by white lines, and the Rayleigh wave speed c_R by a black dashed line.

strain tensor ε_{ij} [see Fig. 1(a)]. In our model, we employ a linear elastic constitutive law, as described by the shear modulus μ and Poisson's ratio ν, to relate the two-dimensional 2nd-Piola-Kirchhoff stress tensor σ_{ij} to E_{ij}, through

$$\sigma_{ij} = 2\mu\left(E_{ij} + \frac{\nu}{1-2\nu}\delta_{ij}E_{kk}\right), \tag{2}$$

where δ_{ij} is the Kronecker delta. Notice that, as sketched in Fig. 1(a), the GNL model ($\alpha = 1$) induces a strain-enhancing effect with respect to the linear case ($\alpha = 0$). The advantage of this model, compared to one with a non-linear constitutive law (e.g., neo-Hookean), is that it allows isolation of the effect of nonlinearity on the crack propagation. In the following, we choose $\mu = 39.2$ kPa and $\nu = 0.35$, and then solve the problem for the conservation of linear momentum (full details provided in [30]).

Fracture of the material is modeled using a cohesive approach, where cohesive tractions across the crack plane represent the progressive failure of the material. In our model, see Fig. 1(a), we adopt a linear cohesive law with $\sigma_c = 20$ kPa and $\Gamma = 15$ J/m^2, which gives a critical opening distance of $\delta_c = 1.5$ mm (for details, see Ref. [30]). This cohesive approach allows for the representation of a cohesive zone that captures localized spatially distributed dissipation, providing an approximation of the process zone observed in natural fractures. We use standard numerical techniques, detailed in [30], to accurately simulate crack growth.

We examine the behavior of fracture growth in a two-dimensional plane-strain system of height $H = 102.6$ mm and length $L = 154$ mm mimicking the most common experimental configuration [see Fig. 1(a)]. The dimensions are chosen sufficiently large to avoid any wave reflections that could affect the results (see Ref. [30]). We apply a uniform and constant remote displacement $\Delta \gg \delta_c$, which results in a uniform stretch $\lambda = 1 + (\Delta/H)$ on the entire sample. We initiate crack growth at time $t = 0$ by artificially introducing a seed crack that slightly exceeds Griffith's critical length for plane-strain conditions given by $L_G = 2\mu\Gamma/\pi(1-\nu)\sigma_\infty^2 = 5.1$ mm where σ_∞ is the applied stress induced by the imposed remote displacement Δ. The growth of the crack is confined to a (weak) plane perpendicular to the imposed stretch and aligned with the seed crack, restricting its propagation to a straight path $y = 0$ [as illustrated in Fig. 1(a)]. This constraint effectively prevents crack branching instabilities, commonly observed [31,32], imitates the grooves used in experiments [28,31], and enables a thorough exploration of crack speeds across the full range.

First, we consider the linear elastic case ($\alpha = 0$). Immediately after the seed crack is introduced, it becomes unstable, accelerates, and propagates through the entire interface [Fig. 1(b), left]. The crack-tip position, as defined by the transition from intact material to the cohesive zone [see Fig. 1(b), left], moves through the interface, leading to a growing crack length $a(t)$. We observe that the crack speed, as computed by $c_f = \mathrm{d}a/\mathrm{d}t$, approaches c_R [see Fig. 1(b), left] but does not exceed it respecting the limiting speed given by LEFM. Considering the exact same model with the sole difference of including geometric nonlinearities ($\alpha = 1$), we observe a different crack propagation [Fig. 1(b), right]. In this case, the crack continuously surpasses both c_R and c_s, and propagates at supershear speeds. These results reveal an unknown mechanism for supershear propagation, which is simply due to geometric nonlinearities.

For a quantitative evaluation of the different crack growth behavior, we consider the instantaneous crack-tip dynamics, as shown in Fig. 2. For uniform systems, LEFM predicts that $c_f/c_R \approx 1 - L_G/a$ (details provided in [30]), which shows that a LEFM-governed crack remains sub-Rayleigh—even if it gets infinitely long. We observe that the simulation with a linear elastic material ($\alpha = 0$) agrees quantitatively well with the LEFM prediction (Fig. 2). Specifically, it asymptotically approaches c_R, satisfying the theoretical limit by remaining at sub-Rayleigh speeds for all crack lengths. In contrast, the simulations with geometric nonlinearities ($\alpha = 1$) do not follow the LEFM prediction and exceed the limiting speed c_R.

These results reveal a few important mechanisms for crack dynamics of geometrically nonlinear materials. First,

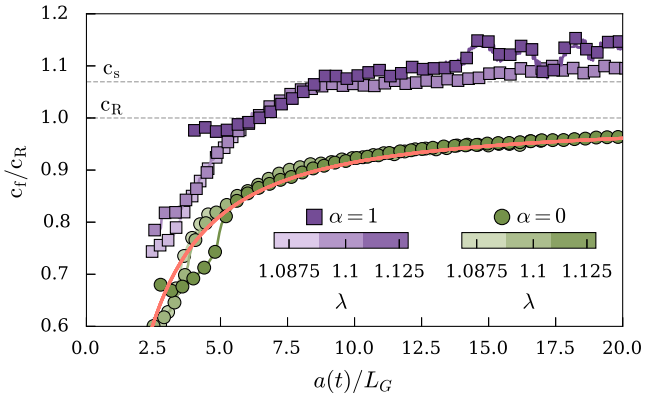

FIG. 2. Crack-tip dynamics for three different values of stretches $\lambda = 1.0875$, 1.1, and 1.125. The crack dynamics are shown in green shades for $\alpha = 0$, and purple shades for $\alpha = 1$, respectively. The red solid line is the LEFM crack-tip equation of motion.

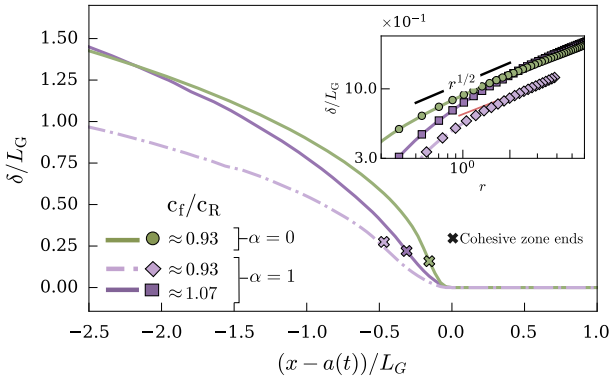

FIG. 3. Crack-tip opening displacement, δ, for simulations at $\lambda = 1.1$ with small strain $\alpha = 0$ (shown in green) and geometric nonlinear strain $\alpha = 1$ (shown in purples). For $\alpha = 1$, the light purple corresponds to the sub-Rayleigh speed, $c_f \approx 0.93 c_R$, and the dark purple corresponds to subsonic speed, $c_f \approx 1.07 c_R$. The cross marks indicate the ends of the cohesive zone. (inset) A log-log plot of δ as a function of $r = (a(t) - x)/L_G$, the distance from the crack tip. The black and red lines indicate $r^{1/2}$ scaling.

simulations at different stretch levels are superimposed when normalized by Griffith's length (see Fig. 2), which suggests that there is a crack-tip equation of motion for geometrically non-linear materials. Second, the crack speeds in the GNL case are consistently and significantly above the LEFM prediction even in the sub-Rayleigh regime (i.e., $c_f < c_R$), indicating that the LEFM energy balance is fundamentally changed. Third, the crack accelerates simply through the transonic speed range $[c_R, c_s]$ to reach supershear speeds ($c_f > c_s$). This is fundamentally different from the sub-Rayleigh–to–supershear transition observed in shear cracks, in which a secondary crack ahead of the main crack is required to allow for a crack speed jump (i.e., discontinuity) across the forbidden transonic speed range [9,12,15].

Next, we focus on the crack-tip opening displacement to determine the mechanisms allowing for propagation through the transonic regime. For the linear case ($\alpha = 0$), see Fig. 3, the crack opening δ follows a square-root behavior outside the cohesive zone, which is, as expected, consistent with LEFM. The GNL material, however, presents a different behavior. Close to the crack-tip (but outside the cohesive zone), the exponent increases (see inset in Fig. 3). This effect becomes even stronger when the crack surpasses c_R (see Fig. 3). These results suggest that the square-root singular behavior of the strain and stress fields is not relevant when GNL effects are considered. This calls into question the foundations of brittle fracture mechanics, which are based mainly on the consequences of the square root behavior for energy budgeting and, thus, for the crack equation of motion. Such an observation may waver one of the fundamental corollaries of LEFM: the maximum speed allowed by the rate of energy flow toward the crack tip.

To visualize further the modified near-tip fields and the associated energy flow to the crack tip, we compute the Poynting vector [4,20] (details in [30]). For the linear material, the Poynting vector field takes the ordinary shape and values [see Fig. 4(a)]. At the same sub-Rayleigh crack speed, the GNL material presents a significantly different pattern [see Fig. 4(b)]. While the magnitude of the Poynting vector is lower in the vicinity of the crack tip (note the absence of blue color), it is somewhat increased further away (see brighter red at $|x| > a$). Further changes occur at transonic crack speeds [see Fig. 4(c)], where the magnitude of the Poynting vector increases but remains below the values observed in the linear material, and the lobes are inclined to the back of the crack, which are forerunners of the Mach cone in the supershear propagation regime [20]. These modifications to the near-tip crack fields confirm that the crack dynamics changed due to the GNL material behavior and point to a totally different energy budgeting even in the subshear propagation regime.

The modified energy flux to the crack tip also causes changes to the local dissipation, which manifests itself in the properties of the cohesive zone. From the near-tip Poynting vector fields [see Figs. 4(a)–4(c)], we observe an increase in the cohesive-zone size $\mathcal{X}(c_f)$ for the GNL case. Quantitatively, the cohesive zone size for the linear material follows, after some initial perturbations from the nucleation, the LEFM prediction [4] with a Lorentz contraction from its static size $\mathcal{X}_0$ to zero towards c_R [see Fig. 4(d)]. In contrast, the cohesive zone in the GNL material is considerably larger and appears to be relatively constant at $\mathcal{X} \approx 0.4\mathcal{X}_0$ while the crack traverses the transonic regime and reaches supershear propagation. This suggests that kinetic energy and bulk wave interference responsible for the Lorentz contraction in LEFM yield completely different results in materials where GNL effects are dominant. The fact that $\mathcal{X}$ is finite in the transonic regime indicates that the

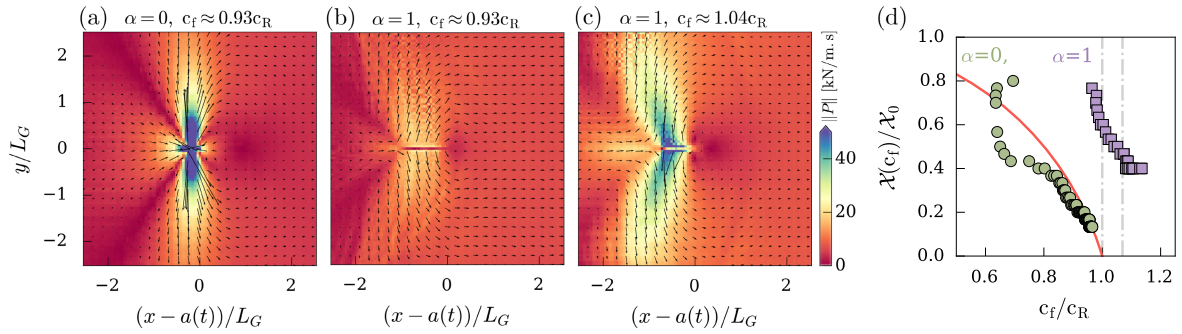

FIG. 4. Snapshots of energy flow density, represented as the magnitude of Poynting vector P_j (see Ref. [30] for more details). All the snapshots are for an imposed stretch $\lambda = 1.125$ (a) $\alpha = 0$ at sub-Rayleigh speed $c_f \approx 0.93 c_R$ (b) $\alpha = 1$ at sub-Rayleigh speed, $c_f \approx 0.93 c_R$ (c) $\alpha = 1$ at subsonic speed, $c_f \approx 1.04 c_R$. (d) Evolution of cohesive zone size $\mathcal{X}(c_f)$ for $\lambda = 1.125$ with small strain $\alpha = 0$ and geometric nonlinear strain $\alpha = 1$. The cohesive zone size is normalized by static cohesive zone size $\mathcal{X}_0$. The red solid line shows the analytical solution for cohesive zone size from LEFM.

Lorentz contraction is superseded by a different mechanism that could be related to either the cohesive zone response or the nonsquare root singular behavior near the crack tip.

The present study confirms previous numerical simulations related to the limiting speed of propagating cracks [20–25]. In MD simulations, where hyperelasticity was assumed, supershear propagation was related to an increased local wave speed in the highly stretched region at the crack tip compared to the far-field wave speed. In simulations using a lattice model, a completely different branch of supershear solutions for propagating cracks was found for stretches above a critical value. However, the novelty of the present work is to show that supershear propagation is possible within a continuum elastic framework. We show that GNL is the principal ingredient to "break" the barrier of Rayleigh wave speed for tensile crack propagation and that there is no forbidden interval velocity. Tensile cracks accelerate smoothly from the sub-Rayleigh regime to the supershear regime. These observations are robust as they do not depend on the specific choice of material parameter values (see Ref. [30]). Moreover, they agree with experiments on crack propagation in hydrogels [28] and rubberlike materials [26,27]. The common thread between our model and these experiments is that the materials considered exhibit a nonlinear elastic response, for which LEFM is possibly not an adequate framework. Note that in the case of hydrogels, experiments show that supershear rupture is enabled above an applied stretch level [28]. We believe that the existence of such a critical stretch is caused by the velocity dependence of the fracture energy of the hydrogel. Our model is consistent with a constant Γ that allows the crack to always be in an accelerating phase (both in LEFM and certainly in GNL frameworks). For GNL simulations, our system size and other crack nucleation aspects prevent us from determining the terminal supershear speed of the crack, which is beyond the scope of this study.

Let us conclude with a discussion on possible directions for future work. The results for the crack-tip opening displacement, energy release rate, and cohesive zone size point toward the conclusion that the elastic field distribution and energy budgeting in the vicinity of the crack tip of a GNL material exhibit completely different behaviors than that of a linear elastic material. Recent attempts to uncover the underlying mechanisms tackled such problems perturbatively [33]; however, our results lean toward a nonperturbative effect. We believe that the methods developed for static cracks in nonlinear materials [34] should be generalized to the dynamic problem. Indeed, important questions arise related to a material's nonlinear response which produces either strain stiffening or strain softening at high stretches. How does it affect our findings and is any nonlinearity capable of allowing supershear cracks? For example, it is believed that dynamic crack growth in a purely neo-Hookean material follows LEFM solutions [33]. How does this reconcile with the fact that the nonlinearity used in our model is present in any material? Why is it believed that supershear crack propagation is not possible in engineering brittle materials such as glass? For this, other instabilities may occur at lower speeds (such as microbranching, oscillatory instabilities, and instabilities along the crack front) prevent cracks from reaching transonic and supershear speeds. Moreover, the brittleness of such materials does not allow them to store enough potential energy prior to crack propagation. This would explain why supershear cracks are commonly associated with direct extreme loading on the crack surface [11,29].

Finally, the classical LEFM theory developed over the last century [4,6] has been a strong backbone for our understanding of material fracture. Here, we demonstrate its breakdown by showing that naturally existing geometric nonlinear strain causes supershear crack propagation, which opens new perspectives in dynamic fracture mechanics.

Note added.—We thank J. Fineberg and M. Wang for sharing their experimental results [28] prior to publication and for fruitful discussions.

D. S. K. and M. P. acknowledge support from the Swiss National Science Foundation under the SNSF starting Grant (TMSGI2_211655).

*dkammer@ethz.ch

[1] T. Baumberger, C. Caroli, and D. Martina, Nat. Mater. **5**, 552 (2006).
[2] H. Bao, L. Xu, L. Meng, J.-P. Ampuero, L. Gao, and H. Zhang, Nat. Geosci. **15**, 942 (2022).
[3] S. Moulinet and M. Adda-Bedia, Phys. Rev. Lett. **115**, 184301 (2015).
[4] L. B. Freund, *Dynamic Fracture Mechanics* (Cambridge University Press, Cambridge, England, 1998), 10.1017/CBO9780511546761.
[5] T. Goldman, A. Livne, and J. Fineberg, Phys. Rev. Lett. **104**, 114301 (2010).
[6] K. B. Broberg, *Cracks and Fracture* (Elsevier, New York, 1999).
[7] R. Burridge, Geophys. J. Int. **35**, 439 (1973).
[8] D. S. Kammer, I. Svetlizky, G. Cohen, and J. Fineberg, Sci. Adv. **4**, eaat5622 (2018).
[9] D. J. Andrews, J. Geophys. Res. (1896–1977) **81**, 5679 (1976).
[10] F. F. Abraham and H. Gao, Phys. Rev. Lett. **84**, 3113 (2000).
[11] A. J. Rosakis, O. Samudrala, and D. Coker, Science **284**, 1337 (1999).
[12] K. Xia, A. J. Rosakis, and H. Kanamori, Science **303**, 1859 (2004).
[13] O. Ben-David, G. Cohen, and J. Fineberg, Science **330**, 211 (2010).
[14] F. X. Passelègue, A. Schubnel, S. Nielsen, H. S. Bhat, and R. Madariaga, Science **340**, 1208 (2013).
[15] I. Svetlizky, D. P. Muñoz, M. Radiguet, D. S. Kammer, J.-F. Molinari, and J. Fineberg, Proc. Natl. Acad. Sci. U.S.A. **113**, 542 (2016).
[16] M. Bouchon and M. Vallée, Science **301**, 824 (2003).
[17] K. T. Walker and P. M. Shearer, J. Geophys. Res. **114**, B02304 (2009).
[18] E. M. Dunham, Bull. Seismol. Soc. Am. **94**, S256 (2004).
[19] D. Wang, J. Mori, and K. Koketsu, Earth Planet. Sci. Lett. **440**, 115 (2016).
[20] M. J. Buehler, F. F. Abraham, and H. Gao, Nature (London) **426**, 141 (2003).
[21] Y. Jia, W. Zhu, T. Li, and B. Liu, J. Mech. Phys. Solids **60**, 1447 (2012).
[22] T. M. Guozden, E. A. Jagla, and M. Marder, Int. J. Fract. **162**, 107 (2010).
[23] L. I. Slepyan, Doklady Akademii Nauk **260**, 566 (1981).
[24] M. Marder, Phys. Rev. Lett. **94**, 048001 (2005).
[25] M. Marder, J. Mech. Phys. Solids **54**, 491 (2006).
[26] P. J. Petersan, R. D. Deegan, M. Marder, and H. L. Swinney, Phys. Rev. Lett. **93**, 015504 (2004).
[27] T.-T. Mai, K. Okuno, K. Tsunoda, and K. Urayama, ACS Macro Lett. **9**, 762 (2020).
[28] M. Wang, S. Shi, and J. Fineberg, Science **381**, 415 (2023).
[29] S. Winkler, D. A. Shockey, and D. R. Curran, Int. J. Fract. Mech. **6**, 151 (1970).
[30] See Supplemental Material at http://link.aps.org/supplemental/10.1103/PhysRevLett.132.226102 for details on the formulation of the numerical framework for modeling dynamic crack propagation in geometrical nonlinear materials, the LEFM equation of motion, and the near-tip Poynting vector field.
[31] P. D. Washabaugh and W. G. Knauss, Int. J. Fract. **65**, 97 (1994).
[32] E. Sharon and J. Fineberg, Nature (London) **397**, 333 (1999).
[33] A. Livne, E. Bouchbinder, I. Svetlizky, and J. Fineberg, Science **327**, 1359 (2010).
[34] R. Long and C.-Y. Hui, Extreme Mech. Lett. **4**, 131 (2015).